Int. J. Solids Structures Vol. 27, No. 2, pp. 205–225, 1991
Printed in Great Britain.

0020-7683/91 $3.00 + .00

STEADY PROPAGATION OF PLANE STRAIN SHEAR CRACKS ON AN IMPERMEABLE PLANE IN AN ELASTIC DIFFUSIVE SOLID

J. W. RUDNICKI and D. A. KOUTSIBELAS
Department of Civil Engineering, Northwestern University, Evanston, IL 60208, U.S.A.

(*Received* 7 *September* 1989; *in revised form* 10 *January* 1990)

Abstract—Quasi-static shear crack propagation in a linear elastic fluid-saturated porous solid causes a change of pore pressure on the crack plane if it is impermeable but not if it is permeable. Assuming that the pore pressure induced on the crack plane reduces the effective compressive stress (total stress minus pore fluid pressure) and, as a result, the frictional resistance, we find that the energy required to drive the crack is decreased by up to about 60% of the value required in a purely elastic solid. The required energy decreases with velocity at low and high velocities, but increases with velocity for Vl/c in the range of $10^{0.5}$–10^{2}, where V is the speed of propagation, l is the loaded length of the semi-infinite crack and c is the diffusivity. When the effect of the pore pressure induced on the crack plane is neglected, the results are qualitatively similar to those of Rice and Simons (1976, *J. Geophys. Res.* **81**, 5322–5344) for the permeable crack: coupling between deformation and diffusion stabilizes propagation in the sense that the energy that must be supplied to drive the crack increases with velocity within a finite range of the ratio Vl/c. This range of Vl/c is about an order of magnitude lower than that for the permeable crack, but includes the range cited above and is within the range of observed creep events on the San Andreas fault.

INTRODUCTION

This paper analyzes the stress and pore pressure fields induced by a plane strain shear (Mode II) crack propagating steadily and quasi-statically in a linear elastic, fluid-infiltrated solid. The response of such a solid, unlike that of an ordinary elastic solid, depends on the time scale of the applied loads. More specifically, the response is stiffer for loads that are applied rapidly by comparison with the time scale of diffusion (undrained conditions) than for loads that are applied slowly enough to allow time for pore pressure equilibration by fluid mass diffusion (drained conditions). Consequently, the stress intensity factor of a crack propagating quasi-statically through a diffusive solid depends on the velocity of propagation. Furthermore, this dependence is different depending on whether the crack plane is permeable or impermeable to the diffusing species.

Consideration of this problem is motivated by applications to the propagation of slip on faults in the Earth's crust. For reasons that will be explained in the body of the paper, previous work on propagating shear cracks in fluid-saturated elastic solids (Rice and Simons, 1976; Simons, 1977; Cleary, 1978) is appropriate when the crack plane is permeable to the diffusing pore fluid. [Hereafter, we will, for brevity, denote the reference Rice and Simons (1976) by RS]. However, faults in the Earth's crust are often thought to be impermeable (Wu *et al.*, 1975; Wang and Lin, 1978) because they contain clay or other fine-grained material. Although slip is not always localized on a discrete plane, intense shear deformation is typically confined to a narrow zone. Hence, for mathematical simplicity, we idealize this zone as an impermeable plane across which the slip displacement can be discontinuous.

The purpose of this paper is to investigate the effects of impermeability of the crack plane on the solution. Recent related work (Rudnicki, 1986, 1987; Rudnicki and Hsu, 1988; Rudnicki and Roeloffs, 1990) has shown that the specification of an impermeable plane can have a significant effect on the stress and pore pressure fields induced by instantaneous and steadily moving shear dislocations.

Previous work on propagating cracks in fluid-infiltrated porous solids (RS; Simons, 1977; Ruina, 1978; Cleary, 1978) has demonstrated that the stiffer response of the fluid-saturated material to rapid deformations can contribute to stabilizing the crack against rapid propagation. RS (also, Rice and Cleary, 1976) have discussed this stabilizing effect

as a possible mechanism for the propagation of creep events (e.g. King *et al.*, 1973; Johnson *et al.*, 1974; Goulty and Gilman, 1978; Evans *et al.*, 1981). These are slip events that propagate too slowly, in the order of 1–10 km per day, to generate seismic radiation. This stabilizing mechanism may also be a factor contributing to the occurrence of slow slip prior to earthquakes. It is possible that such slip could be accompanied by detectable effects that would forecast the impending earthquake (e.g. Rice, 1979a; Rudnicki, 1988).

To make the problem mathematically tractable, we consider the propagation of a semi-infinite shear crack. However, as is well-known from linear elastic fracture mechanics and as discussed by RS, the loading on the semi-infinite crack can be chosen so that the stress field near the edge of the crack is identical to that near a finite crack. To examine the effects of the crack plane impermeability and compare our results with those of RS, we obtain the velocity dependent stress intensity factor for a steadily propagating semi-infinite crack loaded by uniform shear over a finite distance behind its tip. As for the permeable shear crack analyzed by RS, the singular crack-tip model is found to be inadequate at high propagation speeds. Consequently, we also present results for a modification of the Palmer and Rice (1973) cohesive zone model used by RS. This model attempts to account, albeit approximately, for the processes of material breakdown near the crack-tip.

A second effect that occurs for the impermeable fault, but not for the permeable, is due to the change in pore pressure induced on the crack plane. Because the frictional resistance to slip depends on the effective compressive stress, that is, the total compressive stress minus the pore pressure, changes in pore pressure alter the resistance to slip. Although the pore pressure induced on the impermeable crack plane is discontinuous and has opposite signs on the two sides, we argue that the pore pressure increase, which reduces the effective compressive stress and, hence, the frictional resistance, dominates. With this assumption, we estimate the effect of the induced pressure on a criterion for fault propagation and its dependence on the velocity of propagation.

The remainder of the paper begins with a brief discussion of the equations governing the response of a linear elastic diffusive solid. These equations were first formulated by Biot (1941) in the context of fluid-saturated soils and they are formally identical to the equations of fully coupled thermoelasticity (Biot, 1956; Rice and Cleary, 1976; Rice, 1979b). Indeed, they are sufficiently general to describe the linearized response of any elastic solid containing a diffusing species that can be characterized by two scalar variables. The form of the equations to be described here is that introduced by Rice and Cleary (1976).

GOVERNING EQUATIONS

In a linear elastic diffusive solid, two variables, in addition to the strains of the solid matrix ε_{ij} and the total stresses σ_{ij}, are needed to specify the response. These are conveniently taken to be the fluid mass content per unit volume of porous solid m and the pore pressure p. The latter is defined as the pressure, in excess of the ambient, needed to equilibrate any fluid mass flux from small material elements. If the deformation is so slow relative to the time scale of fluid mass diffusion that there is no alteration in pore fluid pressure, $p = 0$ and the response is said to be drained. In this limit the expression for the strain components reduces to the usual one of linear elasticity:

$$2G\varepsilon_{ij} = \sigma_{ij} - [\nu/(1+\nu)]\sigma_{kk}\delta_{ij} \tag{1}$$

where G is the shear modulus, ν is the drained Poisson's ratio and δ_{ij} is the Kronecker delta.

In the contrasting limit of undrained response the deformation is too rapid to allow for fluid mass diffusion from material elements and, hence, m is equal to its reference value m_0. In this case, the alteration in pore fluid pressure is proportional to the negative of the mean normal stress:

$$p = -B\sigma_{kk}/3 \tag{2}$$

where the constant of proportionality B is called Skempton's coefficient. Values of B range

from zero to one with the lower limit attained for highly compressible pore fluid and the upper for separately incompressible solid and fluid constituents. For undrained response, the strains are again related to the stresses by (1) but with ν replaced by ν_u the undrained Poisson's ratio. Since $\nu \leqslant \nu_u \leqslant 1/2$, with limits attained under the same conditions as for the limits of B, the undrained response is stiffer than the drained response.

For arbitrary deformations, the response will be neither drained nor undrained and the expressions for the strains and alteration of m are as follows:

$$2G\varepsilon_{ij} = \sigma_{ij} - [\nu/(1+\nu)]\sigma_{kk}\delta_{ij} + \frac{3(\nu_u - \nu)}{B(1+\nu_u)(1+\nu)} p\delta_{ij} \tag{3}$$

$$m - m_0 = \frac{9\rho_0(\nu_u - \nu)}{2GB(1+\nu_u)(1+\nu)}[\sigma_{kk}/3 + p/B] \tag{4}$$

where ρ_0 is the mass density of homogeneous pore fluid. Rice and Cleary (1976) (also, see Rudnicki, 1985) give a full discussion of the development of these equations and their relation to the formulation of Biot (1941). They also tabulate laboratory values of the parameters ν, ν_u and B. For plane strain deformation in the xy plane, the condition $\varepsilon_{33} = 0$ can be used to eliminate σ_{33} from (3) and (4):

$$2G\varepsilon_{\alpha\beta} = \sigma_{\alpha\beta} - \nu(\sigma_{xx} + \sigma_{yy})\delta_{\alpha\beta} + \frac{3(\nu_u - \nu)}{B(1+\nu_u)} p\delta_{\alpha\beta} \tag{5}$$

$$m - m_0 = \frac{3\rho_0(\nu_u - \nu)}{GB(1+\nu_u)}\left[\frac{1}{2}(\sigma_{xx} + \sigma_{yy}) + \frac{3}{2B(1+\nu_u)} p\right] \tag{6}$$

where, now, $(\alpha, \beta) = (1, 2) = (x, y)$.

The final constitutive equation is Darcy's law (Rice and Cleary, 1976):

$$q_\alpha = -\rho_0 \kappa \, \partial p/\partial x_\alpha \tag{7}$$

where q_α is the mass flow rate in the α direction per unit area and κ is a permeability. The permeability is more frequently expressed in the form $\kappa = k/\gamma$ where γ is the fluid viscosity and k has units of area.

In addition to the constitutive equations (5), (6) and (7) field equations expressing equilibrium, compatibility and fluid mass conservation are needed. The equations of equilibrium in the absence of body forces are as follows:

$$\partial\sigma_{xx}/\partial x + \partial\sigma_{xy}/\partial y = 0 \tag{8}$$

$$\partial\sigma_{xy}/\partial x + \partial\sigma_{yy}/\partial y = 0. \tag{9}$$

The equation of plane strain compatibility can be expressed in terms of the mean stress and pore pressure by means of the usual manipulations:

$$\nabla^2(\sigma_{xx} + \sigma_{yy} + 2\eta p) = 0 \tag{10}$$

where $\nabla^2(\ldots) = \partial^2(\ldots)/\partial x^2 + \partial^2(\ldots)/\partial y^2$ and $\eta = 3(\nu_u - \nu)/[2B(1+\nu_u)(1-\nu)]$. An equation expressing conservation of mass for the fluid constituent is

$$\partial q_\alpha/\partial x_\alpha + \partial m/\partial t = 0. \tag{11}$$

This equation can be rewritten in terms of the stresses and pore pressure by substituting (6) and (7) into (11) and combining with (10):

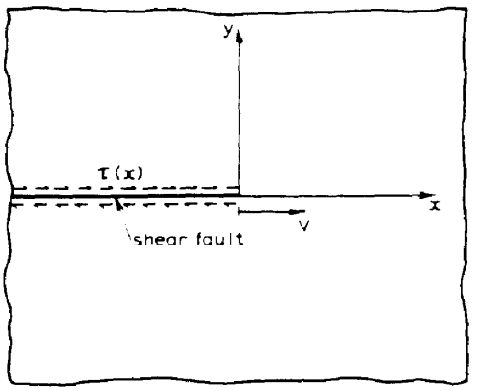

Fig. 1. Coordinate system for a semi-infinite shear fault. The fault moves to the right with a constant speed V under the action of the shear stress $\tau(x)$.

$$(c\nabla^2 - \partial/\partial t)[\sigma_{xx} + \sigma_{yy} + (2\eta/\mu)p] = 0 \tag{12}$$

where $\mu = (\nu_u - \nu)/(1 - \nu)$ and the diffusivity c is given by

$$c = 2G\kappa B^2(1 - \nu)(1 + \nu_u)^2/[9(1 - \nu_u)(\nu_u - \nu)]. \tag{13}$$

Comparison of (12) with (6) reveals that the quantity in square brackets in (12) is proportional to the fluid mass content per unit volume. Hence, as emphasized by Rice and Cleary (1976), m satisfies a homogeneous diffusion equation but the pore pressure p, in general, does not.

The governing eqns (8)–(10) and (12) will be solved for the case of a semi-infinite shear (Mode II) crack located on the x-axis and moving steadily and quasi-statically at a constant speed V (Fig. 1). The crack is loaded by shear stresses $\tau(x)$ which are applied to the crack faces and move with the crack. The crack and the applied loads are assumed to have been moving at this speed long enough so that transient effects have died out. Thus, the problem is one of steady propagation and any explicit dependence on time t can be eliminated by adopting a coordinate system that moves with the crack-tip. Furthermore, for steady propagation in the x direction, $\partial/\partial t$ can be replaced by $-V\partial/\partial x$ and, thus, (12) becomes

$$(c\nabla^2 + V\partial/\partial x)[\sigma_{xx} + \sigma_{yy} + (2\eta/\mu)p] = 0. \tag{14}$$

BOUNDARY CONDITIONS

Because of anti-symmetry about the crack plane $y = 0$, it is possible to formulate the problem in the upper half plane with boundary conditions given on $y = 0$. The stress component σ_{xy} is anti-symmetric about $y = 0$ and, because the normal traction is continuous across $y = 0$, it must be zero there:

$$\sigma_{xy}(x, 0) = 0, \quad -\infty < x < \infty. \tag{15}$$

Similarly, the displacement component u_x is anti-symmetric about $y = 0$. Although u_x is discontinuous on the crack itself, it must be continuous ahead of the crack and, hence, must vanish there:

$$u_x(x, 0) = 0, \quad 0 \leqslant x < \infty. \tag{16}$$

This condition can be rewritten in terms of the stresses and pore pressure by using the strain–displacement relation $\varepsilon_{xx} = \partial u_x/\partial x$ and the constitutive relation (5). The result is

$$\sigma_{xy}(x,0)+2\eta p(x,0)=0, \quad 0 \leqslant x < \infty, \tag{17}$$

where (15) has also been used.

The pore fluid pressure p is also anti-symmetric about $y=0$. Hence, if p is continuous on $y=0$, it must vanish there and (17) reduces to $\sigma_{xy}(x,0)=0$ $(0 \leqslant x < \infty)$. These are the boundary conditions used in previous studies of shear cracks in diffusive solids (RS; Simons, 1977; Cleary, 1978). In this case, $\partial p/\partial y$, in general, will not be zero on $y=0$ and, hence, by Darcy's law (7), fluid will flow across the x-axis. An alternative possibility is that the crack plane models a shear fault that is impermeable to fluid flow. The condition enforcing this requirement is

$$\partial p(x,0)/\partial y=0, \quad -\infty < x < \infty. \tag{18}$$

The pore fluid pressure is still required to be anti-symmetric about $y=0$, but need not be continuous and, hence, takes on equal and opposite values as the x-axis is approached from above or below.

As already mentioned, the applied shear loading on the fault faces is described by $\tau(x)$. This provides the following boundary condition:

$$\sigma_{xy}(x,0) = -\tau(x), \quad -\infty < x \leqslant 0. \tag{19}$$

As discussed by RS, $\tau(x)$ represents the difference between an applied farfield loading and a resistive friction stress. Following RS, we will first solve the problem specified by eqns (8) (10) and (14) and the boundary conditions (15) (19) for a periodic variation of shear stress. Although this loading is of no real interest by itself, it is a basis for developing more realistic solutions by superposition. In particular, we use the result to generate the solution for a uniform distribution of shear stress over a distance l behind the crack-tip.

PERIODIC CRACK FACE LOADING

In this section, we derive the solution for a periodic loading of the crack faces given by

$$\tau(x) = \tau^*(x) = e^{i\kappa x} \tag{20}$$

where $i=(-1)^{1/2}$. With this loading, (19) becomes

$$\sigma_{xy}(x,0) = -e^{i\kappa x}, \quad -\infty < x \leqslant 0. \tag{21}$$

The solution procedure follows that of RS. In particular, we use Fourier transforms and the Wiener–Hopf technique. The Fourier transform of a function $f(x,y)$ is defined as follows:

$$\tilde{f}(\kappa,y) = \int_{-\infty}^{\infty} f(x,y)\, e^{-i\kappa x}\, dx, \tag{22}$$

with inverse

$$f(x,y) = \frac{1}{2\pi}\int_{-\infty}^{\infty} \tilde{f}(\kappa,y)\, e^{i\kappa x}\, d\kappa. \tag{23}$$

Application of (22) to the governing eqns (8)–(10) and (14) yields ordinary differential equations for the transforms of the stress components and pore pressure. The solution to these equations is given by RS as follows:

$$\eta\tilde{p}(\kappa, y) = -\mu A(\kappa) e^{-m(\kappa)y} - B(\kappa) e^{-n(\kappa)y} \tag{24}$$

$$\tilde{\sigma}_{xx}(\kappa, y) = [1 - m(\kappa)y]A(\kappa) e^{-m(\kappa)y} - C(\kappa) e^{-m(\kappa)y} - \frac{2n^2(\kappa)}{\kappa^2 - n^2(\kappa)} B(\kappa) e^{-n(\kappa)y} \tag{25}$$

$$\tilde{\sigma}_{yy}(\kappa, y) = [1 + m(\kappa)y]A(\kappa) e^{-m(\kappa)y} + C(\kappa) e^{-m(\kappa)y} + \frac{2\kappa^2}{\kappa^2 - n^2(\kappa)} B(\kappa) e^{-n(\kappa)y} \tag{26}$$

$$\tilde{\sigma}_{xy}(\kappa, y) = -\left[\iota\kappa y A(\kappa) + \frac{\iota\kappa}{m(\kappa)} C(\kappa)\right] e^{-m(\kappa)y} - \frac{2\iota m(\kappa)}{\kappa^2 - n^2(\kappa)} B(\kappa) e^{-n(\kappa)y} \tag{27}$$

where $m^2(\kappa) = \kappa^2$ and $n^2(\kappa) = \kappa^2 - \iota\kappa V/c$ and $A(\kappa)$, $B(\kappa)$ and $C(\kappa)$ are to be determined. In order to ensure convergence of the inverse transforms in the upper half-plane, $y \geq 0$, $m(\kappa)$ and $n(\kappa)$ are subject to the following restrictions:

$$\mathrm{Re}\,[m(\kappa)] \geq 0, \quad \mathrm{Re}\,[n(\kappa)] \geq 0 \tag{28}$$

where "Re [...]" stands for "the real part of [...]".

Fourier transformation of the boundary conditions (15) and (18) yields

$$\partial\tilde{p}(\kappa, 0)/\partial y = 0 \tag{29}$$

and

$$\tilde{\sigma}_{xy}(\kappa, 0) = 0. \tag{30}$$

Because the two remaining boundary conditions (17) and (21) do not apply on the entire x-axis, the Fourier transforms of the quantities entering these equations are not known completely. Thus, the Fourier transform of the shear stress on $y = 0$ is given by

$$\tilde{\sigma}_{xy}(\kappa, 0) = \int_{-\infty}^{0} \sigma_{xy}(x, 0) e^{\iota\kappa x} dx + F^{-}(\kappa) \tag{31}$$

where the unknown function $F^{-}(\kappa)$ is defined as follows:

$$F^{-}(\kappa) = \int_{0}^{\infty} \sigma_{xy}(x, 0) e^{-\iota\kappa x} dx. \tag{32}$$

As indicated by the superscript, $F^{-}(\kappa)$ is analytic in the lower half of the complex κ plane, i.e. $\mathrm{Im}(\kappa) \leq 0$. Substitution of (21) yields $\iota/(\lambda - \kappa)$ for the first integral in (31), where λ is assumed to have a small negative imaginary part as needed to ensure convergence. Substitution of the expression for $\tilde{\sigma}_{xy}(\kappa, 0)$ from (27) into the left hand side of (31) then gives

$$-\frac{2\iota\kappa n(\kappa)}{\kappa^2 - n^2(\kappa)} B(\kappa) - \frac{\iota\kappa}{m(\kappa)} C(\kappa) = F^{-}(\kappa) - \frac{1}{\iota(\lambda - \kappa)}. \tag{33}$$

Similarly, the Fourier transform of $[\sigma_{yy}(x, 0) + 2\eta p(x, 0)]$ is given by

$$\tilde{\sigma}_{yy}(\kappa, 0) + 2\eta\tilde{p}(\kappa, 0) = G^{+}(\kappa) + \int_{0}^{\infty} [\sigma_{yy}(x, 0) + 2\eta p(x, 0)] e^{\iota\kappa x} dx \tag{34}$$

where

$$G^+(\kappa) = \int_{-\infty}^{0} [\sigma_{xx}(x,0) + 2\eta p(x,0)]\, e^{-i\kappa x}\, dx \tag{35}$$

is analytic in the upper half of the complex κ plane, $\mathrm{Im}(\kappa) \geqslant 0$. The second integral in (34) vanishes because of (17) and use of (24) and (25) to evaluate the left-hand side yields:

$$(1-2\mu)A(\kappa) - \frac{2\kappa^2}{\kappa^2 - n^2(\kappa)} B(\kappa) - C(\kappa) = G^+(\kappa). \tag{36}$$

The functions A, B and C can be expressed in terms of $G^+(\kappa)$ by using (24) and (25) to evaluate (29) and (30) and solving the resulting equations along with (36). The results are as follows:

$$A(\kappa) = \frac{G^+(\kappa)}{2(1-\mu)} \tag{37}$$

$$B(\kappa) = -\frac{\mu m(\kappa) G^+(\kappa)}{2(1-\mu)n(\kappa)} \tag{38}$$

$$C(\kappa) = -\frac{G^+(\kappa)}{2(1-\mu)} \left\{ 1 + (2i\kappa c/V) \frac{m(\kappa)}{n(\kappa)} \right\}. \tag{39}$$

Substitution of (37) (39) into (33) then gives

$$\frac{G^+(\kappa)}{2(1-\mu)} \left\{ \frac{i\kappa}{m(\kappa)} - (2\mu c/V)\, m(\kappa) \left[\frac{m(\kappa)}{n(\kappa)} - 1 \right] \right\} = F^-(\kappa) + \frac{1}{i(\kappa - \lambda)}. \tag{40}$$

This is a typical Wiener Hopf equation (Noble, 1958) that relates the two unknown half-range transforms $G^+(\kappa)$ and $F^-(\kappa)$. The solution procedure involves rearranging the equation so that each side is an analytic function of κ in half-planes of the complex κ plane. If the half-planes overlap, then each side of the equation is a representation of the same entire function. To this end, we follow RS and express $m(\kappa)$ and $n(\kappa)$ as products of functions analytic in the upper and lower half-planes:

$$m(\kappa) = m^+(\kappa) m^-(\kappa), \quad n(\kappa) = n^+(\kappa) n^-(\kappa). \tag{41}$$

The function $m^+(\kappa) = \kappa^{1/2}$ has a branch cut on the negative imaginary axis and, hence, is analytic in $\mathrm{Im}(\kappa) > 0$. Similarly, $m^-(\kappa)$ has a branch cut on the positive imaginary axis from $i\varepsilon$ to $i\infty$, where ε is a small positive constant that eventually will be made to approach zero, and is analytic in $\mathrm{Im}(\kappa) < \varepsilon$. The function $n^-(\kappa) = (\kappa - iV/c)^{1/2}$ has a branch cut on the positive imaginary axis from iV/c to $i\infty$. Note that this choice of branch cuts is consistent with the restrictions (28), that $[m^+(\kappa)]^2 = \kappa^2$, and that $[m^-(\kappa)]^2 = \kappa^2$ in the limit $\varepsilon \to 0$.

The relations (41) can be used to rewrite (40) as follows:

$$\frac{iG^+(\kappa)}{2m^+(\kappa)} = \frac{F^-(\kappa)}{m^-(\kappa) D^-(\kappa)} + \frac{1}{i(\kappa - \lambda) m^-(\kappa) D^-(\kappa)} \tag{42}$$

where

$$D^-(\kappa) = \frac{1}{1-\mu} \left\{ 1 + (2i\kappa\mu c/V) \left[\frac{m^-(\kappa)}{n^-(\kappa)} - 1 \right] \right\}. \tag{43}$$

Because $n^-(\kappa)$ is never equal to zero for $\mathrm{Im}(\kappa) \leqslant 0$ (as long as $V > 0$) $D^-(\kappa)$ is analytic for

$\mathrm{Im}(\kappa) \leqslant 0$ and, in fact, for $\mathrm{Im}(\kappa) \leqslant \varepsilon$. Furthermore, $D^-(\kappa) \neq 0$ in the lower half-plane, approaches $1/(1-\mu)$ as $|\kappa| \to 0$, and approaches 1 as $|\kappa| \to \infty$.

The left hand side of (42) is analytic in the upper half-plane but the right hand side still has a pole in the lower half-plane at $\kappa = \lambda$ (Recall that λ has a small negative imaginary part). However, the right hand side can be made analytic by subtracting an appropriate term from both sides. The result is the desired rearrangement:

$$\frac{iG^+(\kappa)}{2m^+(\kappa)} - \frac{1}{i(\kappa-\lambda)m^-(\lambda)D^-(\lambda)} = \frac{F^-(\kappa)}{m^-(\kappa)D^-(\kappa)} + \frac{1}{i(\kappa-\lambda)}\left[\frac{1}{m^-(\kappa)D^-(\kappa)} - \frac{1}{m^-(\lambda)D^-(\lambda)}\right]. \quad (44)$$

Now, the left-hand side is analytic for $\mathrm{Im}(\kappa) > 0$, the right-hand side is analytic for $\mathrm{Im}(\kappa) < 0$ and the two sides are identical on the real κ axis. Thus, each side of (44) is the analytic continuation of the other and both are equal to an entire function, say $H(\kappa)$.

The function $H(\kappa)$ can be determined from the asymptotic behavior of (44). Because of the requirements of bounded strain energy, both $G^+(\kappa)$ and $F^-(\kappa)$ approach zero as $|\kappa| \to \infty$. As a result, both sides of (44) tend to zero as $|\kappa| \to \infty$ in the appropriate domain of analyticity. By means of Liouville's theorem (e.g. Carrier *et al.*, 1966), we can conclude that $H(\kappa)$ is identically zero in the entire κ plane. Equating the left hand side of (44) to zero yields

$$G^+(\kappa) = -\frac{2m^+(\kappa)}{(\kappa-\lambda)m^-(\lambda)D^-(\lambda)}. \quad (45)$$

Substitution into (37)–(39) yields expressions for A, B and C. In principle, the solutions for the pore pressure and stress components can be obtained by substituting the results for A, B and C into (24)–(27) and using the Fourier inversion (23). For example, the shear stress σ_{xy} is given by

$$\sigma_{xy}(x,y) = \frac{1}{2\pi(1-\mu)m^-(\lambda)D^-(\lambda)}\int_{-\infty}^{\infty}\frac{1}{(\kappa-\lambda)}\left\{e^{m(\kappa)y}\left[\frac{i\kappa}{m(\kappa)} - i\kappa y\right] - (2\mu c/V)\left[m(\kappa)e^{m(\kappa)y} - \frac{\kappa^2}{m(\kappa)}e^{m(\kappa)y}\right]\right\}e^{i\kappa x}\,d\kappa \quad (46)$$

Although the integrals in (46) cannot be expressed in closed form, it is possible to evaluate them as $r \to 0$, where $r = (x^2+y^2)^{1/2}$. The basic strategy is to transform the integrals to contours in the complex κ plane on which the exponents are real and negative. Approximation for small r then leads to the asymptotic expression:

$$\sigma_{xy} = \frac{K}{(2\pi r)^{1/2}}\cos(\theta/2)\,[1 - \sin(\theta/2)\sin(3\theta/2)] + O(1) \quad (47)$$

where

$$K = \frac{1-\mu}{m^-(\lambda)D^-(\lambda)} \quad (48)$$

is the stress intensity factor for the loading $\tau^{(\infty)}(x) = e^{i\lambda x}$. The expression for σ_{xy} is identical in form to the field near a Mode II crack in a linear elastic solid (Rice, 1968), but, of course, here the stress intensity factor K depends on the velocity and diffusivity. The result for the stress intensity factor (48) has the same form as that obtained by RS for the permeable fault, but differs in the expression for $D^-(\lambda)$.

Similarly, the other stress components can be shown to approach the form of the linear elastic crack-tip field as $r \to 0$. Asymptotic evaluation of the pore pressure is more formidable. Because of cancelling terms the calculation requires considerable care. A more direct approach is to use a boundary layer analysis of the governing equations (Simons, 1977; Rudnicki, 1990). By either method, it can be shown that the pore pressure is bounded and finite as $r \to 0$.

Later, we will also need the expression for the slip $\delta(x)$ on the crack which, because of anti-symmetry, is equal to $2u_y(x, 0^-)$. Use of the strain displacement relation $\varepsilon_{xx} = \partial u_x/\partial x$ and the constitutive relation (5) leads to the following expression for the slip on $x \leqslant 0$:

$$\delta(x) = [(1-\nu)/G] \int_0^x [\sigma_{xx}(x, 0) + 2\eta p(x, 0)]\, \mathrm{d}x. \tag{49}$$

Inversion of (34) and substitution of (45) yields

$$\delta(x) = \frac{1-\nu}{\mathrm{i}\pi G m^-(\lambda) D^-(\lambda)} \int_{-\infty}^{+\infty} [(1-\mathrm{e}^{\mathrm{i}\kappa x})/m^+(\kappa)(\kappa-\lambda)]\, \mathrm{d}\kappa. \tag{50}$$

This integral can be evaluated as described by RS and, again, the result is identical in form to theirs but with a different expression for D^-:

$$\delta(x) = \frac{2(1-\nu)\, \mathrm{e}^{\mathrm{i}\pi/4} \operatorname{erf}[\mathrm{e}^{-\mathrm{i}\pi/4} m^-(\lambda) |x|^{1/2}]}{G\lambda D^-(\lambda)} \tag{51}$$

where $\operatorname{erf}(\xi)$ is the error function (Abramowitz and Stegun, 1964).

UNIFORM SHEAR LOADING OVER A DISTANCE l

The solution obtained in the last section can be used to develop the solution for any arbitrary loading by Fourier superposition. Let $f^{(\lambda)}$ denote any field quantity, for example, stress or pore pressure, due to the loading $\tau^{(\lambda)}(x) = \mathrm{e}^{\mathrm{i}\lambda x}$. Then, the corresponding quantity due for arbitrary loading $\tau(x)$ is given by

$$f(x, y) = (1/2\pi) \int_{-\infty}^{+\infty} \tilde{\tau}(\lambda)\, f^{(\lambda)}(x, y)\, \mathrm{d}\lambda \tag{52}$$

where $\tilde{\tau}(\lambda)$ is the Fourier transform (22) of $\tau(x)$ with λ denoting the transform variable.

In this section, we use this procedure to obtain the stress-intensity factor for uniform shear loading over a distance l behind the crack edge:

$$\tau(x) = (\tau_a - \tau_f) H(x+l), \quad x < 0, \tag{53}$$

where $H(x)$ is the Heaviside step function. As explained by RS, this is a simple model of a shear fault. The loading is the difference between an applied shear stress τ_a that arises from large-scale tectonic forces and a resistive friction stress τ_f, assumed here to be constant. RS also note that although the fault is assumed to be semi-infinite for mathematical simplicity, the distance l can be adjusted so that the elastic stress field near the fault edge is the same as that for a finite length fault.

The Fourier transform of the loading (53) is

$$\tilde{\tau}(\lambda) = -(\tau_a - \tau_f)(1 - \mathrm{e}^{\mathrm{i}\lambda l})/\mathrm{i}\lambda. \tag{54}$$

Applying (52) to the expression for the stress intensity factor (48) and using (54) yields

$$K = \frac{-(1-\nu)}{2\pi\iota}(\tau_a - \tau_f)\int_{-\infty}^{+\infty} \frac{1-e^{-\lambda\iota}}{\lambda m^-(\lambda)D^-(\lambda)}\,d\lambda. \tag{55}$$

This equation can be rewritten in the form

$$K = K_{nom}h(Vl/c) \tag{56}$$

where

$$K_{nom} = (\tau_a - \tau_f)(8l/\pi)^{1/2} \tag{57}$$

is the stress intensity factor for an elastic solid subjected to the same loading and

$$h(Vl/c) = -\frac{e^{-\pi i/4}}{4\iota\pi^{1/2}}\int_{-\infty}^{+\infty} \frac{1-e^{s}}{s\hat{D}^-(s, Vl/c)m^-(s)}\,ds \tag{58}$$

is a real-valued dimensionless factor. The functions $\hat{D}^-(s,\gamma)$ and $m^-(s)$ are given as follows:

$$\hat{D}^-(s,\gamma) = \beta + [2\iota s(\beta-1)/\gamma]\left[\frac{m^-(s)}{n^-(s,\gamma)} - 1\right] \qquad m^-(s) = s^{1/2}, \tag{59}$$

where

$$n^-(s,\gamma) = (s-\iota\gamma)^{1/2}, \quad \beta = (1-\nu)/(1-\nu_u). \tag{60}$$

As suggested by the notation, the functions $m^-(s)$ and $n^-(s,\gamma)$ have their branch cuts on the positive imaginary axis of the complex s plane and are defined to have positive real parts when $s > 0$. By means of the same manipulations used by RS, the integral (58) can be transformed to a form more suitable for numerical evaluation:

$$h(\gamma) = \frac{1}{2\pi^{1/2}}\int_0^{\infty} \psi^{1/2}(1-e^{-\psi})\,\mathrm{Re}\left[\frac{1}{\hat{D}_r^-(\iota\psi,\gamma)}\right]d\psi, \tag{61}$$

where $\hat{D}_r^-(\iota\psi,\gamma)$ is the limit of $\hat{D}^-(s,\gamma)$ as s approaches the point $\iota\psi$ ($\psi > 0$) from the right on the complex s plane.

It can easily be shown that $h(Vl/c)$ approaches one for $Vl/c \to 0$. This result is expected because, for very slow propagation, there is ample time for any excess pore pressures to be dissipated by fluid diffusion and the material responds in drained fashion. Hence, the stress intensity factor is identical to that in an ordinary elastic body and $K = K_{nom}$. In the contrasting limit of $Vl/c \to \infty$, $h(Vl/c)$ approaches $\beta^{-1} = (1-\nu_u)/(1-\nu) < 1$. (Because $\nu_u \geqslant \nu$, $\beta \geqslant 1$.) RS rationalize this result in terms of the compatibility of deformation between a region near the crack-tip responding in drained fashion and a surrounding undrained region. Simons (1977) has given a more precise interpretation by means of a boundary layer analysis.

The integral (61) is identical to that found by Ruina (1978) in the problem of a steadily propagating opening (Mode I) crack. For tensile loading the condition (18) arises from the symmetry of the problem and, in this case, the pore pressure is continuous across the fault plane. The coincidence of (61) with the result of Ruina (1978) means that if the crack plane is impermeable, the velocity dependence of the stress intensity factor is the same whether the loading is tensile or shear. Corresponding features have been noted in solutions for instantaneous (Rudnicki, 1987) and steadily propagating (Rudnicki and Roeloffs, 1990) plane strain dislocations. Consequently the feature seems to be general although we know of no demonstration of this.

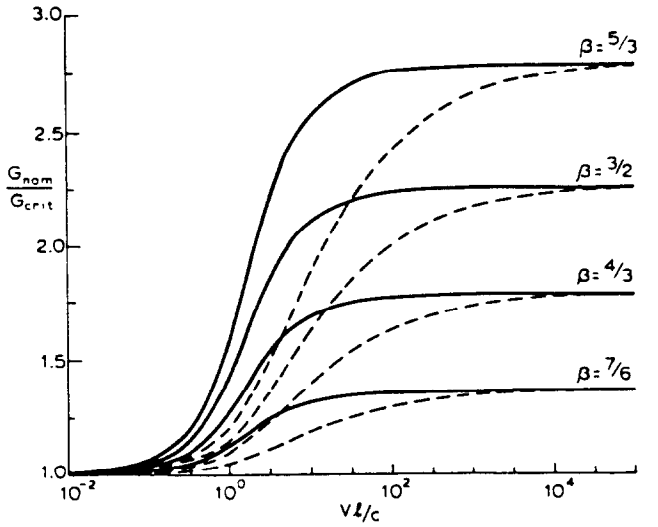

Fig. 2. A plot of the fault propagation criterion $G_{nom}h^2(Vl/c) = G_{crit}$ based on the singular crack-tip model (63) for various values of $\beta = (1-\nu)/(1-\nu_u)$. The results of Rice and Simons (1976) for the permeable fault are shown dashed. The values of G_{nom}/G_{crit} approach β^2 for large Vl/c.

Thus far, we have assumed that both the speed of propagation V and the driving stress on the crack faces $\tau_a - \tau_f$ can be prescribed independently. However, in actuality, the speed at which the fault propagates will depend on the driving stress. A simple criterion that relates these quantities is that the fault propagates when the elastic energy released per unit advance of the crack G_{rel} reaches some critical value, say, G_{crit}. The value of G_{crit} is presumed to be characteristic of the material and independent of the geometry and loading conditions. Although this criterion takes no specific account of the actual processes of material breakdown near the crack-tip, it is a good approximation when the size of this breakdown zone is small compared with other dimensions of the problem, that is, for small scale yielding conditions (See, e.g. Rice, 1968). However, as in the case of the permeable fault, we will find that at larger propagation speeds predictions based on this criterion become suspect because the diffusion length c/V approaches the size of the breakdown zone. In this case, a more elaborate model of the breakdown process is required.

The energy release rate is related to K by the following well-known expression (Irwin, 1960; Rice, 1968):

$$G_{rel} = K^2(1-\nu)/2G. \tag{62}$$

Hence, substituting (56) and setting $G_{rel} = G_{crit}$ for propagation yields

$$G_{nom}/G_{crit} = [h(Vl/c)]^{-2} \tag{63}$$

where G_{nom} is defined by substituting K_{nom} into (62). G_{nom} is the energy release rate for a crack propagating in an ordinary elastic solid and, as a result, represents the energy supplied by the applied loads.

The ratio (63) is plotted in Fig. 2 for the range of values of β considered by RS. For example, the combination of $\nu = 0.2$ and $\nu_u = 0.4$ leads to $\beta = 4/3$ which, according to RS, is reasonable for a fissured rock mass, whereas they suggest a value of $\beta = 5/3$ as more appropriate for clay soils. For comparison, the results of RS for the permeable shear crack are shown as dashed lines. Figure 2 shows that for any value of β, the ratio G_{nom}/G_{crit} is an increasing function of the dimensionless speed measure Vl/c and hence of V. Because G_{crit} is assumed to be constant, this means that an increase in the propagation speed requires an increase in G_{nom} and, hence, in the driving stress $\tau_a - \tau_f$. Consistent with the behavior of K, G_{nom}/G_{crit} approaches one as $V \to 0$ and approaches β^2 as $V \to \infty$.

FAULT SPREADING CRITERION BASED ON PALMER RICE MODEL

As already noted, the fracture criterion based on a critical value of the energy release rate is appropriate when small scale yielding conditions prevail, that is, when the inelastic deformation accompanying the micromechanical processes of relative sliding occurs in a zone that is smaller than all other characteristic lengths in the problem. However, as the speed of propagation V increases, the characteristic diffusion length c/V will eventually become comparable to the size of this breakdown zone. In this case the singular crack-tip model is no longer valid. Consequently, we follow RS and consider the Palmer and Rice (1973) model which incorporates a finite size zone of breakdown processes at the crack tip and is similar to cohesive zone models of tensile cracks (e.g. Dugdale, 1960; Barenblatt, 1962). Detailed explanations of the model have been given by Palmer and Rice (1973) and by RS. Summaries are contained in review articles by Rice (1980, 1983) and Rudnicki (1980, 1988).

The Palmer and Rice (1973) cohesive zone model has two main features. The first is that shear stresses τ_b, in excess of τ_f, resist relative slip in a zone behind the crack-tip $-\omega \leqslant x \leqslant 0$. These stresses oppose the driving stresses in such a way that the singular stress at the crack tip is eliminated. The stress τ_b arises from the micromechanical processes resisting relative slip and, in general, depends on the local slip. However, for simplicity, we take τ_b as constant. Therefore, as explained in more detail by RS, the loading is the sum of that given by (53) and the following:

$$\tau(x) = -(\tau_b - \tau_f), \quad -\omega \leqslant x \leqslant 0, \tag{64}$$

where the minus sign enters because τ_b resists slip. Because the stress intensity factor for uniform loading behind the crack-tip is given by (56) with (57), the condition that the singularity at the crack-tip vanish is simply the following:

$$(\tau_a - \tau_f)(8l/\pi)^{1/2} h(Vl/c) - (\tau_b - \tau_f)(8\omega/\pi)^{1/2} h(V\omega/c) = 0, \tag{65}$$

where $h(\gamma)$ is given by (61). This equation relates the driving stress $\tau_a - \tau_f$ to the breakdown zone size ω, but is insufficient to determine the amount of slip required for the slip zone to advance.

The second feature of the Palmer and Rice (1973) model is that advance of the slip zone occurs when the slip at the trailing edge of the breakdown zone is equal to a critical value δ_{crit}:

$$\delta(x = -\omega) = \delta_{crit}. \tag{66}$$

In order to implement this condition, it is necessary to calculate the slip induced by the sum of the loadings (53) and (64). This is accomplished by employing the procedure summarized by (52) with the generic function f replaced by δ and $\delta^{(2)}$ given by (50). Thus, the slip caused by the loading (54) is given by

$$\delta(x) = \frac{(1-\nu)(\tau_a - \tau_f)l}{G} g(|x|/l, Vl/c), \quad x < 0 \tag{67}$$

where the function g is an integral defined in obvious fashion by use of (51) and (54) in (52). As in RS, this expression for g is not very convenient for numerical evaluation and the manipulations described by them are used to arrive at the following more suitable representation:

$$g(\alpha, \gamma) = \frac{2}{\pi} \int_0^\infty \{2(\alpha\psi/\pi)^{1/2} - e^{-(1-i)\sqrt{\alpha\psi}} \operatorname{erf}[(\alpha\psi)^{1/2}]\} \operatorname{Re}\left[\frac{1}{\psi^2 \hat{D}_r(i\psi, \gamma)}\right] d\psi. \tag{68}$$

The sliding displacement $\delta(x)$ caused by the sum of the loadings (53) and (64) is obtained by simple superposition, and the result of imposing (66) is the following:

$$\delta_{crit} = \frac{1-\nu}{G}\left[(\tau_a-\tau_f)lg\left(\frac{\omega}{l},\frac{Vl}{c}\right)-(\tau_b-\tau_f)\omega g\left(1,\frac{V\omega}{c}\right)\right]. \tag{69}$$

It is, however, more convenient to express this criterion in terms of the parameters arising in the singular crack-tip model. Palmer and Rice (1973) have shown that their model provides an explicit interpretation for G_{crit} as the energy, in excess of that dissipated by the residual friction resistance τ_r, required to advance the fault a unit distance:

$$G_{crit} = \int_0^{\delta_{crit}} [\tau(\delta)-\tau_r]\,d\delta. \tag{70}$$

In the simple model employed here, the shear stress in the endzone is a constant τ_b and (70) reduces to

$$G_{crit} = (\tau_b-\tau_f)\delta_{crit}. \tag{71}$$

Equations (71) and (65) can be used to rearrange (69) as follows:

$$\frac{G_{nom}}{G_{crit}} = \frac{4h^2(V\omega/c)}{\pi h(Vl/c)[(l/\omega)^{1/2}h(V\omega/c)g(\omega/l, Vl/c)-h(Vl/c)g(1, V\omega/c)]} \tag{72}$$

where G_{nom} is defined as before as the energy release rate for a crack in an elastic body (without an endzone).

The two eqns (65) and (72) can, in principle, be solved to determine the endzone size ω and the driving stress $\tau_a-\tau_f$. For simplicity, however, we again follow RS and evaluate (72) for a range of fixed values of ω/l. Endzone sizes appropriate for faults *in situ* are not known with much certainty but they are generally thought to be small. Summaries of values inferred from laboratory and field observations have been given by Rice (1979a, 1980, 1983) and Li (1987). In Fig. 3, we have plotted the ratio G_{nom}/G_{crit}, as in (72), as a function of Vl/c for $\omega/l = 10^{-4}$, 10^{-3}, 10^{-2} and 10^{-1}. The results shown are for $\beta = (1-\nu)/(1-\nu_u) = 4/3$. For the lower values of ω/l, which are of greater practical interest, the ratio of G_{nom}/G_{crit} approaches rapidly the value 1 as Vl/c goes to zero. This is expected since at

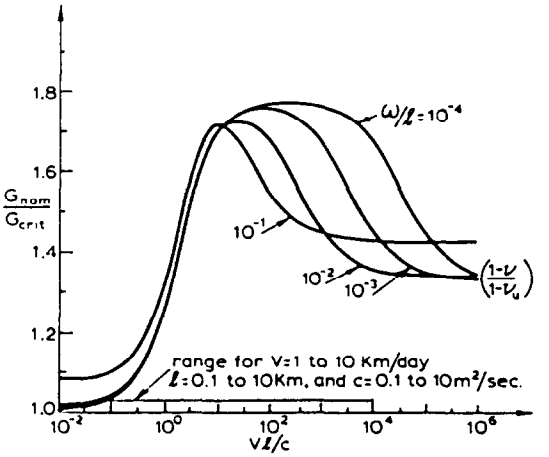

Fig. 3. The fault propagation criterion based on the Palmer and Rice (1973) cohesive zone model (72) for various ratios of the endzone size ω to fault length l. The curves shown are for $\beta = 4/3$. As shown, the curves approach β for large values of Vl/c. The range of Vl/c that corresponds to observed fault creep events, as explained in the text, is also indicated.

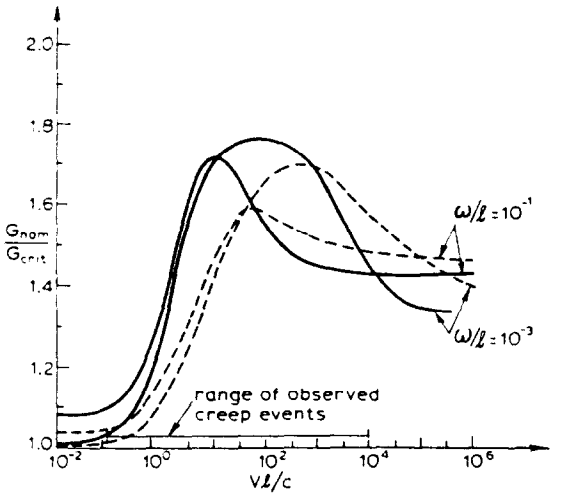

Fig. 4. A comparison of the cohesive zone fault propagation criterion (72) for the permeable (dashed) and impermeable faults. The curves are shown for $\beta = 4/3$ and two values of ω/l, where ω is the endzone size and l is the fault length.

the lower speed limit the response is completely drained (there is no excess pore pressure) and the porous material behaves exactly as an elastic solid with shear modulus G and Poisson's ratio ν (drained). On the other hand, at the higher speed limit, the response is undrained since there is not enough time for the dissipation of the excess pore pressure. The material then behaves elastically with the same shear modulus G but with the undrained Poisson's ratio ν_u. A simple calculation reveals that G_{nom}/G_{crit} approaches the value $\beta = (1-\nu)/(1-\nu_u)$ as V goes to infinity, as indicated in Fig. 3.

For intermediate values of Vl/c, the behavior of G_{nom}/G_{crit}, in contrast to the behavior in the absence of an endzone, is not a monotonic function of Vl/c. More specifically, the ratio attains a maximum at some intermediate value of Vl/c which depends on the ratio ω/l. This maximum value is different for each ω/l and, for small values of ω/l, approaches β^2, which is the maximum value in the absence of the endzone. The shape of the curves in Fig. 3 suggests that for propagation speeds less than that corresponding to the maximum value of G_{nom}/G_{crit} fault propagation is stable because an increase in the driving force is needed to make the fault spread faster. Beyond the peak of the curve, increases in propagation speed occur with diminishing values of the driving force. Thus, the calculations predict that quasi-static spreading is no longer possible and unstable dynamic propagation occurs. The inclusion of a finite endzone size in the analysis results in a finite range of speeds for which the coupled deformation–diffusion effects discussed here stabilize propagation.

The results for the impermeable fault are compared to those of RS for the permeable fault in Fig. 4. This figure plots G_{nom}/G_{crit} against Vl/c for two values of ω/l, 10^{-1} and 10^{-3}, and $\beta = 4/3$. Although the results are qualitatively similar, there are differences in the magnitude of the stabilizing effect and the range of values of Vl/c over which it occurs. Consider, for example, the pair of curves corresponding to $\omega/l = 10^{-3}$. At the peaks of the curves, the values of G_{nom}/G_{crit} are comparable, 1.69 for the permeable fault and 1.76 for the impermeable. But the value of Vl/c at which the peak occurs for the permeable fault, about 10^{1}, is an order of magnitude larger than the corresponding value for the impermeable fault. Over the common rising portion of the two curves, Vl/c less than about 10^{2}, the values of G_{nom}/G_{crit} are significantly higher, as much as 27%, for the impermeable fault than for the permeable. Hence, for this range of Vl/c, the stabilizing effects of coupling between deformation and diffusion are more pronounced for the impermeable fault than for the permeable. This result can be rationalized qualitatively as follows: the geometry of the problem tends to cause pore fluid to flow across the fault plane; this is possible for the permeable fault, but for the impermeable, the pore fluid is forced to seek other less favorable paths. Consequently, the energy needed to drive the fault at the same speed is greater for the impermeable fault.

Observations of creep events for which both the slip length l and the speed of propagation V have been measured are scarce. In Figs 3 and 4 we have indicated a range of observed creep events based on RS's discussion of observations by King *et al.* (1973). They cite slip lengths between 0.1 and 10 km and speeds mostly in the range of 1–10 km per day with one event at 80 km per day. Roeloffs and Rudnicki (1984) summarize, in their Table 1, observations by Evans *et al.* (1981) and Goulty and Gilman (1978) of other episodic creep events for which the propagation speed and slip length were measued. Slip lengths were in the same range, 0.1–10 km, but propagation speeds were somewhat higher, from about 0.8 to 48 km per day. Values of the diffusivity in the vicinity of faults are uncertain and a summary of values by Rudnicki (1984) spans three orders of magnitude, from 0.01 to 10.0 $m^2\ s^{-1}$. RS use a value of $c = 1.0\ m^2\ s^{-1}$ and, with l and V in the range noted above, the corresponding range of Vl/c is $1–10^{-3}$. Because of uncertainty in the value of c, we have indicated a larger range of $0.1–10^{-4}$.

PORE PRESSURE INDUCED ON THE FAULT PLANE

A major difference between shear crack propagation on permeable and impermeable planes is the change in pore pressure induced on $y = 0$. For the permeable plane, there is no change in pore pressure on $y = 0$; for the impermeable, the pore pressure takes on values that are equal in magnitude and opposite in sign as $y = 0$ is approached through positive and negative values. Change in pore pressure on the crack plane affects slip by altering the frictional resistance. More specifically, induction of pore pressure alters the effective compressive stress to which the residual friction stress is proportional. Experimental observations (e.g. Paterson, 1978) and theoretical considerations (Rice, 1977) suggest that the appropriate form of the effective stress for frictional sliding is the difference between the total compressive stress and the pore pressure. Hence, the effective shear stress on the fault becomes

$$\tau(x) = \tau_a - \tau_f + \phi[\sigma_{yy}(x, 0) + p(x, 0)] \tag{73}$$

where ϕ is a coefficient of friction and τ_a and τ_f are the values at ambient normal stress and pore pressure. [Because of (15), the total normal stress is zero on $y = 0$.]

As the pore pressure is discontinuous on $y = 0$, the frictional resistance decreases on the side of the crack for which the pore pressure increases ($y = 0^+$ for the loading and geometry assumed here) and decreases on the other side. Although the positive and negative contributions might be thought to cancel, we argue, following a suggestion of Rice (personal communication, 1987), that the pore pressure increase, causing a decrease in frictional resistance, is of greater significance in affecting propagation: because the impermeable crack idealizes a narrow, but finite thickness, fault zone, the pore pressure within the zone will vary rapidly but continuously between the values $p(x, 0^+)$ and $p(x, 0^-)$ predicted from the solution for the impermeable plane. If it is assumed that slip localizes on a surface within the narrow fault zone, it is plausible that propagation will follow the path of least resistance within the fault zone and hence tend to propagate on the side where the pore pressure increases and the frictional resistance decreases. Although observational evidence that slip localizes to a surface within the fault zone is not clear, continuum solutions for localization of deformation in materials with constitutive relations representaive of rock suggest that this will be the case, e.g. Rudnicki and Rice (1975), Rudnicki (1977).

Including the alteration of the frictional resistance by the induced pore pressure in a rigorous manner is a formidable problem. Because the pore pressure alters the effective loading as indicated by (73), the techniques used in the preceding sections to calculate the stress intensity factor and energy release rate are no longer applicable and numerical methods are required *ab initio*. Consequently, we examine the effects of the induced pore pressure on propagation independently of the coupled deformation–diffusion effects that have already been considered. More specifically, we calculate the pore pressure induced on $y = 0^+$ by the loading (53) and then estimate the effect on the propagation criterion by calculating the stress intensity factor due to the augmented loading (73). This procedure is

similar to that used by Rice (1973, 1980) to calculate the stabilizing effect of suctions induced by dilation in the endzone of a propagating shear band or shear fault.

The pore pressure induced by the loading (53) could be calculated by the procedure summarized by eqn (52). But because the pore pressure induced by the periodic loading (21) cannot be expressed in finite form, application of this technique is awkward. Consequently, we use a different, though approximate, approach that takes advantage of a recent result by Rudnicki and Roeloffs (1990) for the pore pressure induced by a plane strain shear (gliding edge) dislocation propagating steadily on an impermeable plane. Rudnicki and Roeloffs (1990) give the following expression for the pore pressure induced on $y = 0^+$ by a dislocation of unit magnitude (the pore pressure on $y = 0^-$ is equal in magnitude and opposite in sign)

$$p^{\mathrm{dis}}(x, 0^+) = \frac{G(V/c)\mu}{4(1-\nu_u)\eta} P(Vx/2c) \tag{74}$$

where

$$P(\xi) = \exp(-\xi)\{I_0(\xi) - I_1(\xi)\} \tag{75}$$

and I_0 and I_1 are modified Bessel functions of orders zero and one, respectively (Abramowitz and Stegun, Section 9.6, 1964). The expression (74) applies for $x \geqslant 0$; the pore pressure is identically zero for $x < 0$. Therefore, by means of the standard procedures for superposing dislocations (Rice, 1968; Bilby and Eshelby, 1968), the pore pressure induced by a sliding discontinuity $\delta(x)$, for $x < 0$, is

$$p(x, 0^+) = -\int_{-\infty}^{x} H(\quad) \frac{\partial \delta}{\partial \xi}(\xi)\, p^{\mathrm{dis}}(x-\xi)\, \mathrm{d}\xi \tag{76}$$

where $H(x)$ is the Heaviside step function and the form of the upper limit takes advantage of the vanishing of $\delta(x)$ for $x \geqslant 0$ and of $p^{\mathrm{dis}}(x, 0^+)$ for $x < 0$.

For $\delta(x)$ we use the slip induced by the loading (53) in a cracked elastic solid with undrained Poisson's ratio (Rice, 1968; RS):

$$\delta(x) = \frac{4(1-\nu_u)}{\pi G} (\tau_a - \tau_f) l f(|x|/l) \tag{77}$$

where

$$f(\lambda) = \lambda^{1/2} - \tfrac{1}{2}(1-\lambda)\log\frac{[1+\lambda^{1/2}]}{|1-\lambda^{1/2}|}. \tag{78}$$

The expression (77) with (78) is actually the difference between the displacement due to a singular crack-tip field with K given by (57) and that due to the loading (53). Hence, there is no stress singularity at the crack-tip, $x = 0$, as appropriate for an endzone that is much smaller than the crack length l. The use of the undrained Poisson's ratio provides a lower bound on the actual slip; an upper bound is obtained by replacing ν_u by ν. Hence, the ratio of the bounds is $\beta = (1-\nu)/(1-\nu_u)$.

Substitution of (77), with (78), into (76) and a change of integration variable yield the following expression for the pressure on $y = 0^+$ arranged in non-dimensional form:

$$\frac{\pi\eta p(x, 0^+)}{2\mu(\tau_a - \tau_f)} = \Sigma(x/l, Vl/c) \tag{79}$$

where

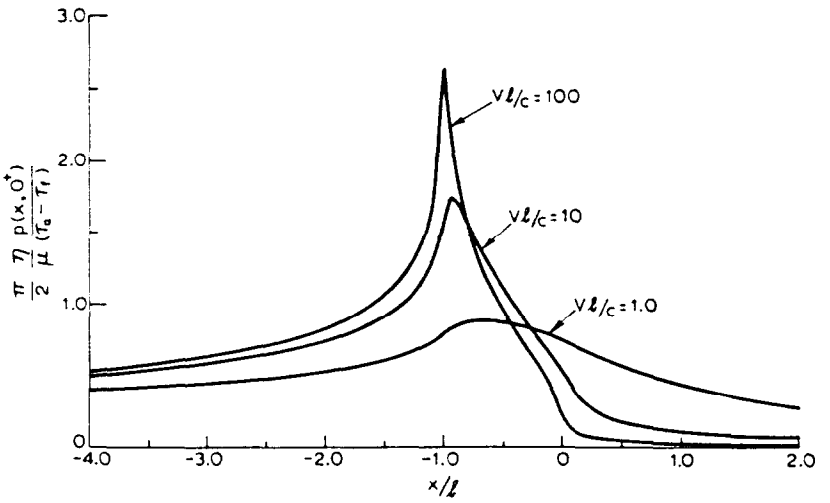

Fig. 5. Pressure, in nondimensional form (79), induced on the impermeable plane for three values of $V\ell/c$. Plot is for $y = 0^+$; values for $y = 0^-$ are equal in magnitude and opposite in sign.

$$\Sigma(x/l, V l/c) = (V l/2c) \int_{(|x|-l)/l(c\ \ v)}^{t} f'(u) P[(V l/2c)(u + x/l)]\, du, \tag{80}$$

$f'(u) = df/du$ and $P(\xi)$ is given by (75). Figure 5 plots the left hand side of (79) against x/l for three values of $V l/c$, 1, 10, 100, the middle of the range representative of field conditions. As shown, the maximum pore pressure increase occurs at $x = -l$, the trailing edge of the loaded portion of the crack faces and increases with $V l/c$. The pressure decreases rapidly with x ahead of the crack-tip, $x > 0$, at least for $V l/c$ greater than unity, and more slowly for $x < -l$. For $V l/c$ greater than about 10, the maximum pore pressure change is proportional to the logarithm of $V l/c$.

The magnitude of the pore pressure change, expressed as a percentage of the stress difference $\tau_a - \tau_f$, depends on the factor $2\mu/\pi\eta$. Rice and Cleary (1976) have inferred and tabulated values of the porous media parameters entering (3) and (4). For the six rock types they consider, the ratio μ/η ranges from 0.43 to 0.76 and, for reasons discussed by Rice and Rudnicki (1979), the upper end of this range is probably more appropriate to field conditions. For these values of μ/η, the ratio $2\mu/\pi\eta$ ranges from 0.27 to 0.48. For $V l/c = 10.0$, the left hand side of (79) is 1.6 for $x = -l$ and, consequently, $p(-l, 0^+)$ is 43–77% of $\tau_a - \tau_f$. If the drained Poisson's ratio is used in (77), values are larger by a factor of β. For $V l/c$ an order of magnitude larger and smaller, the values differ by factors of 1.6 and 0.50, respectively. Thus, the maximum pore pressure change can be a significant fraction of the driving stress $\tau_a - \tau_f$. However, the stress intensity factor depends not only on the maximum pressure change but also on the distribution.

The stress intensity factor K due to a loading $\tau(x)$ applied to a semi-infinite crack is given by

$$K = \frac{2}{\pi^{1/2}} \int_{-\infty}^{0} \frac{\tau(x)}{(-x)^{1/2}}\, dx. \tag{81}$$

Substitution of (73) yields

$$K = K_{\text{nom}}\{1 + k(V l/c)\} \tag{82}$$

where

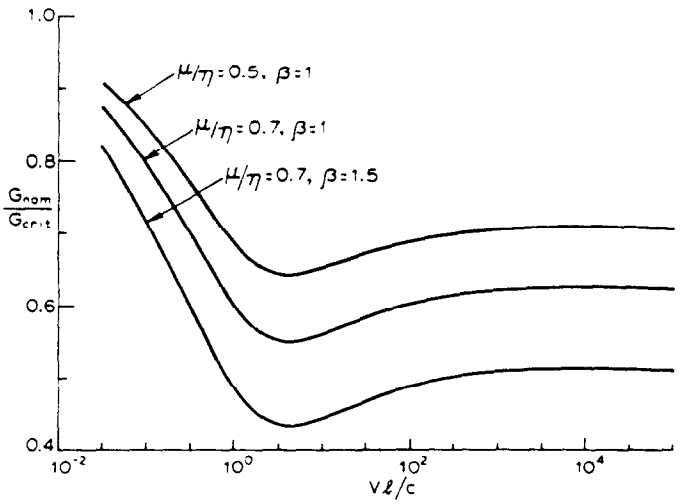

Fig. 6. Effect of the pressure on the fault spreading criterion (85). Curves are shown for two values of μ/η. $\beta = 1$ yields an upper bound corresponding to the use of the undrained slip distribution in (77); $\beta = 1.5$ yields a lower bound corresponding to the use of the drained slip distribution.

$$k(Vl/c) = \left[\frac{2}{l}\right]^{1/2} \frac{\phi\mu}{\pi\eta} \int_{-l}^{0} \Sigma(x/l; Vl/c) \frac{dx}{(-x)^{1/2}} \tag{83}$$

is the contribution from the pressure and K_{nom} is given by (57). Because of the slow decay of Σ as $x \to -\infty$ ($\Sigma \propto (-x)^{-1/2}$), the integral is, however, formally divergent and it is necessary to replace the lower limit by some finite value. Consistent with the interpretation of l as the fault length, we take $-l$ to be the lower limit. With this replacement and a change of variable, $k(Vl/c)$ becomes

$$k(Vl/c) = \frac{(2)^{1/2}\phi\mu}{\pi\eta} \int_{0}^{1} \Sigma(-s; Vl/c) \frac{ds}{s^{1/2}}. \tag{84}$$

Application of (62) to obtain the corresponding energy release rate and imposition of the criterion $G_{rel} = G_{crit}$ yields

$$\frac{G_{nom}}{G_{crit}} = \frac{1}{[1+k(Vl/c)]^2}. \tag{85}$$

Figure 6 plots G_{nom}/G_{crit} against Vl/c for $\mu/\eta = 0.7$ and 0.5, which are near the upper and lower ends of the range for six rock types tabulated by Rice and Cleary (1976), and a friction coefficient of $\phi = 0.6$. In contrast to the previous results, G_{nom}/G_{crit} is less than one because the increase in pressure augments the stress intensity factor and decreases the driving stress needed to propagate the crack at a given velocity. For example, for $\mu/\eta = 0.7$ and $Vl/c = 100$, the energy required to drive the crack is only about 60% of that needed to drive the crack in an elastic solid and, hence, the required value of $\tau_a - \tau_f$ is smaller by a factor of 0.77 ($= 0.60^{1/2}$). Recall that the use of the undrained Poisson's ratio in (77) yields a lower bound on the induced pressure and, correspondingly, an upper bound on G_{nom}/G_{crit}. Figure 6 also shows the result for $\mu/\eta = 0.7$ and $\beta = 1.5$, corresponding to the use of ν in (77). For $Vl/c = 100$, G_{nom}/G_{crit} is reduced from 0.60 to 0.49.

The dependence of G_{nom}/G_{crit} on velocity can be rationalized in terms of the behavior of the induced pressure: although the maximum pressure increases with velocity, Fig. 5 indicates that the region of significant pressure increase becomes more concentrated at $x = -l$ as the velocity increases. Because the effect of the pressure on the stress intensity factor depends on the pressure induced on $-l \leqslant x \leqslant 0$ weighted by the inverse square root

factor, the narrowing of the distribution eventually overcomes the increase in pressure. Hence, for Vl/c between about $10^{0.5}$ and 10^4 G_{nom}/G_{crit} increases with velocity. For still larger values of Vl/c, the ratio decreases slowly.

CONCLUDING DISCUSSION

We have examined coupled deformation diffusion effects in the steady propagation of a plane strain shear crack on an impermeable plane in a porous fluid-infiltrated solid. This investigation is complementary to and uses, for the most part, the same methods as the analysis by RS of shear crack propagation on a permeable plane.

When the effect of the pore pressure induced on the impermeable plane in diminishing the frictional resistance is neglected, the results for the impermeable plane are qualitatively similar to those for the permeable. In particular, coupling between deformation and diffusion is stabilizing in the sense that the energy that must be supplied by the applied loads to drive the crack at a given velocity increases with velocity. For a simple model in which the stress at the crack-tip is singular, the energy that must be supplied increases monotonically with velocity and the ratio of the necessary energy to drive the crack at infinite velocity to that for zero velocity is β^2. When a more detailed model of crack-tip processes that includes a breakdown zone is used, the range of Vl/c for which coupled deformation diffusion effects are stabilizing is finite. Thus, this analysis for an impermeable plane, like that of RS for a permeable plane, predicts that there is a maximum velocity for which these effects are stabilizing. The predicted maximum velocity is reasonably consistent with observations although there is considerable uncertainty in the parameters, particularly the diffusivity.

Although the results for the impermeable plane are similar to those for the permeable, there are significant quantitative differences. Specifically, for Vl/c less than about 100, the stabilizing effects are greater, by as much as 27%, for the impermeable plane. Moreover, the range of Vl/c for which stabilization occurs is about an order of magnitude lower for the impermeable plane.

More dramatic difference between the impermeable and permeable cases results from the alteration of pore pressure on the impermeable fault plane. The change in pore pressure alters the effective compressive stress (total compressive stress minus pore pressure) which in turn affects the frictional resistance. The results indicate that the magnitude of the maximum pressure change on the fault can be a significant fraction, 0.43–0.77, of the driving stress. If one accepts the path of least resistance argument that suggests pore pressure increases, which reduce the frictional resistance, are more significant in affecting propagation, then this effect is destabilizing in the sense that the pore pressure increases the effective driving stress. The calculations suggest that the nominal energy release rate required to drive the crack can be reduced by 50% or more by comparison with that needed in a purely elastic solid. Although the induced pore pressure reduces the required driving stress, the ratio G_{nom}/G_{crit} increases by about 14% as Vl/c increases from $10^{0.5}$ to 10^2. Thus, because an increase in driving stress is needed to drive the crack at higher velocities within this range, the induced pore pressure contributes to the stabilizing effects even though the value of G_{nom}/G_{crit} is less than that for a purely elastic solid.

For simplicity, the two effects of the coupling between deformation and diffusion, the stiffer response of the material surrounding the crack to rapid deformation and the alteration of the frictional resistance by pore pressure induced on the crack, have been studied separately. In actuality, they occur simultaneously and are coupled. Determining the extent to which the increase of G_{nom}/G_{crit} due to the first effect may offset the decrease due to the second requires further study. An additional stabilizing effect, which has not been considered here, can result from dilation accompanying shear (Rice, 1973, 1980; Rudnicki and Chen, 1988). Finally, this paper has emphasized coupling between deformation and pore fluid diffusion as a possible mechanism for episodic creep events but it is important to acknowledge that a variety of other mechanisms have also been suggested. These include time and rate dependence of friction, the coupling of the elastic crust to a more viscous substrate, and the viscoelastic response of fault zone materials.

Acknowledgements—We thank Jim Rice, Andy Ruina and Don Simons for helpful discussions. This work was supported by N.S.F. Grant EAR-8511536.

REFERENCES

Abramowitz, M. and Stegun, I. A. (Eds) (1964). *Handbook of Mathematical Functions*. *Appl. Math. Ser.* **55**. National Bureau of Standards, Washington, DC.

Barenblatt, G. I. (1962). Mathematical theory of equilibrium cracks in brittle fracture. *Adv. Appl. Mech.* **7**, 55–129.

Bilby, B. A. and Eshelby, J. D. (1968). Dislocations and the theory of fracture. In *Fracture: An Advanced Treatise* (Edited by H. Liebowitz), Vol. 1, pp. 99–182. Academic, New York.

Biot, M. A. (1941). General theory of three-dimensional consolidation. *J. Appl. Phys.* **12**, 155–164.

Biot, M. A. (1956). Thermoelasticity and irreversible thermodynamics. *J. Appl. Phys.* **27**, 240–253.

Carrier, G. F., Krook, M. and Pearson, C. E. (1966). *Functions of a Complex Variable*. McGraw-Hill, New York.

Cleary, M. P. (1978). Moving singularities in elasto-diffusive solids with applications to fracture propagation. *Int. J. Solids Structures* **14**, 81–97.

Dugdale, D. S. (1960). Yielding of steel sheets containing slits. *J. Mech. Phys. Solids* **8**, 100–104.

Evans, K. F., Burford, R. O. and King, G. C. P. (1981). Propagating episodic creep and the aseismic slip behavior of the Calaveras fault north of Hollister, California. *J. Geophys. Res.* **86**, 3721–3735.

Goulty, N. R. and Gilman R. (1978). Repeated creep events on the San Andreas fault near Parkfield, California, recorded by a strainmeter array. *J. Geophys. Res.* **83**, 5415–5419.

Irwin, G. R. (1960). Fracture mechanics. In *Structural Mechanics* (Edited by J. N. Goodier and N. J. Hoff), pp. 557–592. Pergamon, New York.

Johnson, A. G., Kovach, R. L. and Nur, A. (1974). Fluid-pressure variations and fault creep in central California. *Tectonophysics* **23**, 257–266.

King, C.-Y., Nason, R. D. and Tocher, D. (1973). Kinematics of fault creep. *Phil. Trans. R. Soc. Lond., Ser. A* **274**, 355–360.

Li, V. C. (1987). Mechanics of shear rupture applied to earthquake zones. In *Rock Fracture Mechanics and Geophysics* (Edited by B. Atkinson). Academic Press, New York.

Noble, B. (1958). *Methods Based on the Wiener–Hopf Technique*. Pergamon, New York.

Palmer, A. C. and Rice, J. R. (1973). The growth of slip surfaces in the progressive failure of overconsolidated clay. *Proc. R. Soc. Lond. Ser. A* **332**, 527–548.

Paterson, M. S. (1978). *Experimental Rock Deformation—The Brittle Field*. Springer, New York.

Rice, J. R. (1968). Mathematical analysis in the mechanics of fracture. In *Fracture: An Advanced Treatise* (Edited by H. Liebowitz), Vol. 2, pp. 191–311. Academic, New York.

Rice, J. R. (1973). The initiation and growth of shear bands. In *Plasticity and Soil Mechanics* (Edited by A. C. Palmer), pp. 263–274. Cambridge University Engineering Department, Cambridge, England.

Rice, J. R. (1977). Pore pressure effects in inelastic constitutive formulations for fissured rock masses. In *Advances in Civil Engineering through Engineering Mechanics*, pp. 360–363. American Society of Civil Engineers, New York.

Rice, J. R. (1977). Personal communication.

Rice, J. R. (1979a). Theory of precursory processes in the inception of earthquake rupture. *Gerlands Beitr. Geophys.* **88**, 91–127.

Rice, J. R. (1979b). The mechanics of quasistatic crack growth. In *Proc. 8th U.S. Nat. Congr. Appl. Mech.* (Edited by R. E. Kelly), pp. 191–216. Western Periodicals, North Hollywood, CA.

Rice, J. R. (1980). The mechanics of earthquake rupture. In *Physics of the Earth's Interior, Proc. Int. School Physics "Enrico Fermi"* **78**, (Edited by A. M. Dziewonski and E. Boschi), pp. 555–649. North Holland, Amsterdam.

Rice, J. R. (1983). Constitutive relations for fault slip and earthquake instabilities. *Pure Appl. Geophys.* **121**, 443–475.

Rice, J. R. and Cleary M. P. (1976). Some basic stress diffusion solutions for fluid-saturated elastic porous media with compressible constituents. *Rev. Geophys. Space Phys.* **14**, 227–241.

Rice, J. R. and Rudnicki, J. W. (1979). Earthquake precursory effects due to pore fluid stabilization of a weakening fault zone. *J. Geophys. Res.* **84**, 2177–2193.

Rice, J. R. and Simons D. A. (1976). The stabilization of spreading shear faults by coupled deformation–diffusion effects in fluid-infiltrated porous materials. *J. Geophys. Res.* **81**, 5322–5344.

Roeloffs, E. and Rudnicki, J. W. (1984). Coupled deformation–diffusion effects on water-level changes due to propagating creep events. *Pure Appl. Geophys.* **122**, 560–582.

Rudnicki, J. W. (1977). The inception of faulting in a rock mass with a weakened zone. *J. Geophys. Res.* **82**, 844–854.

Rudnicki, J. W. (1980). Fracture mechanics applied to the earth's crust. *Annual Rev. Earth Planet Sci.* **8**, 489–525.

Rudnicki, J. W. (1984). Effects of dilatant hardening on the development of concentrated shear deformation in fissured rock masses. *J. Geophys. Res.* **89**, 9259–9270.

Rudnicki, J. W. (1985). Effect of pore fluid diffusion on deformation and failure of rock. In *Mechanics of Geomaterials* (Edited by Z. Bazant), pp. 315–347. Wiley, New York.

Rudnicki, J. W. (1986). Slip on an impermeable fault in a fluid-saturated rock mass. In *Earthquake Source Mechanics* (Edited by S. Das, J. Boatwright and C. H. Scholz), pp. 81–89. American Geophysical Union, Geophysical Monograph 37.

Rudnicki, J. W. (1987). Plane strain dislocations in linear elastic diffusive solids. *J. Appl. Mech.* **54**, 545–552.

Rudnicki, J. W. (1988). Physical models of earthquake instability and precursory processes. *Pure Appl. Geophys.* **126**, 531–554.

Rudnicki, J. W. (1990). Boundary layer analysis of a plane strain shear crack propagating on an impermeable plane in a linear diffusive solid. To appear in *J. Mech. Phys. Solids*.

Rudnicki, J. W. and Chen, C.-H. (1988). Stabilization of rapid frictional slip on a weakening fault by dilatant hardening. *J. Geophys. Res.* **93**, 4745–4757.

Rudnicki, J. W. and Hsu T.-C. (1988). Pore pressure changes induced by slip on permeable and impermeable faults. *J. Geophys. Res.* **93**, 3275–3285.

Rudnicki, J. W. and Rice, J. R. (1975). Conditions for the localization of deformation in pressure-sensitive dilatant materials. *J. Mech. Phys. Solids* **23**, 371–394.

Rudnicki, J. W. and Roeloffs, E. A. (1990). Plane strain shear dislocations moving steadily in linear elastic diffusive solids. *J. Appl. Mech.* **57**, 32–39.

Ruina, A. (1978). Influence of coupled deformation–diffusion effects on retardation of hydraulic fracture. In *Proc. 19th U.S. Symp. Rock Mech.* Stateline, NV. (Edited by Y. S. Kim), pp. 274–272.

Simons, D. A. (1977). Boundary-layer analysis of propagating Mode II cracks in porous elastic solids. *J. Mech. Phys. Solids* **25**, 99–116.

Wang, C.-Y. and Lin, W. (1978). Constitution of the San Andreas fault zone at depth. *Geophys. Res. Lett.* **5**, 741–744.

Wu, F. T., Blatter, L. and Roberson, H. (1975). Clay gouges in the San Andreas fault system and their possible implications. *Pure Appl. Geophys.* **113**, 87–95.